Numerical Simulation of Micro-Pattern Gaseous Detectors

A *project report* submitted by

Danush S

Supervised by

Prof. Supratik Mukhopadhyay,

Saha Institute of Nuclear Physics, Kolkata

July - September, 2020

Acknowledgments

I thank Prof. Supratik Mukhopadhyay for providing me the opportunity to work under his guidance for this project and for the time he spent on this project when most professors were skeptical of taking students for internships during the pandemic., This project has been a tremendous factor into shaping my further interests in research. The entire project was done through an online mode owing to the constraints set by the COVID-19 pandemic. All throughout the project, Prof. Supratik has been patient, open-minded and also supportive to new ideas.

I would also like to thank Vishal Kumar for also guiding me throughout this project, from whom I also learnt some simple tricks to make code faster. I thank Prof. Bedangadas Mohanty and Dr. Varchaswi K. S. Kashyap for allowing me to access NISER's computers for using COMSOL Multiphysics®, without their permission this part of the project would have been disrupted. I would also thank Dr. Abhik Jash, Soumik Chandra, and Aman Upadhyay their help and motivation they have provided me. Finally, and definitely equally important as the above acknowledgments, I thank my parents, family and friends for their support.

Abstract

This project involves studying and running simulations of the neBEM solver in Garfield++. Important concepts related to neBEM are discussed and then simulations using the same were done for the Thick-Gaseous Electron Multiplying detector. We compared our results with an industry standard FEM solver, COMSOL Multiphysics®. Then, our focus shifted to simulating electric fields for different meshes of the Micromegas (with calendared meshes) and Bulk Micromegas detectors. Simulations of these configurations was also carried out on COMSOL Multiphysics® to compare it with the electric field values obtained using neBEM. Although not completed owing to time constraints, we also sought to find the expected gain and signals in one of these mesh configurations of the Micromegas detector. This process involved successfully simulating the drift lines produced for an incoming muon.

List of Figures

List of Tables

Contents

Chapter 1

Introduction

There are multiple ways to simulate microscopic processes of a detector (especially gaseous detectors) used in High Energy Physics experiments. Depending on the requirements of an experiment, there is also a need to study or simulate the electrostatic fields of a detector beforehand to provide us with information as to what configuration to use in the experiment. Once information regarding the electric field is obtained, one can proceed to simulate the processes that occur in a detector to obtain information like gain, signal,resolution, etc. There are again different ways to simulate these microscopic processes, and further details on the same will be discussed in subsequent sections.

We can broadly classify this project into two parts: obtaining electric field information and plotting drift lines (and calculating other values like signal and gain) for two detectors, namely the Thick-Gas Electron Multiplier (Thick-GEM) and the Micromegas detector. The objective to perform these studies was to provide enough information to design the detector that would be made at Saha Institute of Nuclear Physics, Kolkata. Further details on the specifics will be discussed as we progress through the report.

A crucial objective in most nuclear or particle physics experiments is the detection of the radiation/particles that are emitted. It is thus important to look at how different particles and radiation interact with matter. This is one of the basis upon which detector designs are done. The variety of these processes is quite extensive and as a consequence, a large number of detection devices for particles and radiation exist. Depending on the energy of the incident radiation/particle, there are various methods for detection. A lot of advances have been made towards these detectors, and we will briefly go through some relevant detectors in this chapter, studying their structural design and the physics behind them.

1.1 Energy Loss of Particles Passing Through Matter

In the case of gaseous detectors, information regarding the energy lost by an incident particle while it traverses through the gas is important. The Bethe-Bloch equation describes the energy loss (through many interactions) that heavy-charged particles like alpha particles

undergo while traversing through a medium. There are also corrections to use the equation for light-charged particles like protons and electrons. The equation is as follows:

$$-\frac{dE}{dx} = 2\pi N_{\mathrm{a}} r_{\mathrm{e}}^2 m_{\mathrm{c}} c^2 \rho \frac{Z}{A}\frac{z^2}{\beta^2}\left[\ln\left(\frac{2m_e\gamma^2 v^2 W_{\max}}{I^2}\right) - 2\beta^2 - \delta - 2\frac{C}{Z}\right] \tag{1.1}$$

where r_e and m_e are the radius and mass of an electron respectively, N_a is the Avogadro's number, I is the mean excitation potential, Z, A and ρ are the atomic number, atomic weight and density of the medium respectively, z and v are the charge and velocity of the incident particle respectively, δ and C are the density and shell correction terms respectively and W_{max} is the maximum energy transfer possible in a single collision (obtained from kinematics).

Ref. [1] succinctly goes through the ins and outs of the Bethe-Bloch equation, the situations where this equation fails and when can it be used.

1.2 Interaction of Charged and Neutral Particles

Charged particles, as the name hints, are involved in electromagnetic interactions with the gas particles. Upon interaction with a charged particle, gas particles can undergo radiationless rearrangements, dissociate or get excited or ionized, with the emission of photons or the appearance of free ion-electron pairs. At very high particle energy, other mechanisms like Bremsstrahlung and Cherenkov radiation can occur. Electrons and photons created by the primary encounters can further interact with the gas molecules, causing further ionizations called secondary ionizations. Charged particles can also undergo mechanical elastic collisions, and the slowing down in gas is mainly due to multiple inelastic processes of excitation and ionization.

Neutrons are particles with no charge and hence are not involved in any electromagnetic interaction with charged particles. But they can interact with other nuclei through processes like radioactive capture and nuclear reactions with the emission of particles (like protons, alpha particles, etc.) take place. Neutrons also interact with matter through elastic and inelastic scattering.

1.3 Interaction of Photons

The interaction of photons with matter happen majorly through the Photoelectric effect, the Compton Effect and the Pair-Production Effect. Depending on the properties like the incident energy of the photon, the cross sections of each of these processes vary.

The photoelectric effect refers to the emission of electrons when a photon interacts with it. It occurs when the energy of the incident photon is higher but around the magnitude of the ionization energy of the atom. Sometimes the photon can eject an inner shell electron followed by rearrangement of electrons in the atom producing another photon or electron during the process.

Compton effect occurs when the energy of the incident photon is to some extent greater than the ionization energy of the atom. It is the process of transferring some of the energy and momentum to an electron the photon collides with.

The Pair-Production effect is observed when the incident photon is of energy greater than twice the mass of an electron. Pair production often refers to a photon creating an electron-positron pair near a nucleus.

The above interactions should cover a majority of possible interactions, but things get complicated when the medium does not comprise of just single atoms, but a mixture of atoms and molecules. For example in molecular gases, energy can also be spent in rotational, vibrational energy, etc. An account of more than 20 processes that can follow the inelastic interaction of electrons and molecules are provided in Ref. [2].

1.4 Brief Account of Gaseous Detectors

The working principle behind gaseous detectors involves detecting incoming particles by producing a readable electric current through ionization of the gas particles. The particles we wish to detect enters the gaseous detector, ionizes the atoms/molecules of the medium and produces one or more primary ion-electron pairs depending on factors like the energy of the incident particle. Due to the external electric field, usually, these electrons accelerate and gain enough energy to create secondary interactions and produce more ion-electron pairs. Under these conditions, the number of electrons grows rapidly forming an avalanche multiplication (also called as the Townsend Avalanche), thus producing a readable electric signal on the electrodes [3]. There are different innovative designs of gaseous detectors to achieve the above characteristics. One of the early ones was the Multi-Wire Proportional Chamber which consisted of a set of thin, parallel and equally spaced anode wires, symmetrically placed between two cathode planes. Another example is the Micro-Strip Gas Counter that has an upper drift electrode and thin parallel metal strips, alternating wide (anodes) and narrow (cathodes) laid on an insulating support usually at a pitch of a few hundred microns. Schematic diagrams of the same are as seen in Figures 1.1a and 1.1b. Since our simulations involve the Thick-Gas Electron Multiplier (Thick-GEM) and Micromegas detectors, the following subsections goes into brief description of detectors.

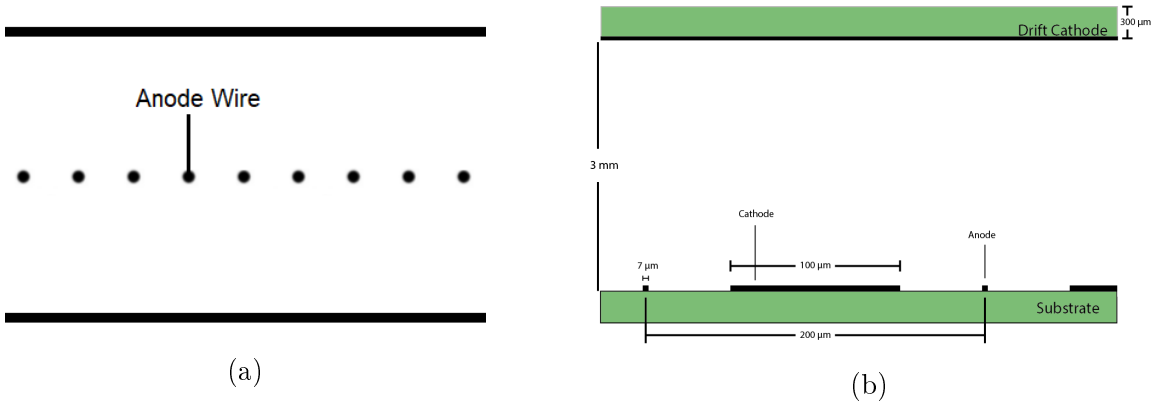

(a) (b)

Figure 1.1: Schematic diagram of a (a) Multi-Wire Proportional Counter and a (b) Micro-Strip Gas Counter. Source: [4]

1.4.1 The Thick-GEM Detector

The Thick-GEM detector is in some ways an improvement of the GEM detector where the delicacy of the foil was undesirable. The Thick-GEM is physically more durable with the ability to sustain electrical discharges. It also gives a much higher gain, making it easy to read the currents. But GEMs offer better spatial resolution than compared to Thick-GEMs. The Thick-GEM foil is made of PCB board (the PCB material, usually FR4, is generally around 0.4-0.8mm thick, but thicker materials are used in research) with copper clads on both side. The board is perforated by holes of a cylindrical shape (usually with a diameter of 0.5mm), and these holes can be mechanically drilled, which makes it cheaper to make than compared to GEMs (which need etching techniques). High voltages are applied on both copper surfaces to provide for a high voltage gradient. The electric field across the Thick-GEM electrode is generally around 25kV/cm. The foil is placed in between a drift electrode and readout pads (anode), all in an air-tight environment with a specific gas or combination of gases. Electrons deposited by the incident ionizing radiation in the drift region, drift towards the Thick-GEM foil under the drift field and then are focused into the dipole field within the micron-hole. The shape of the hole ensures a high dipole field and a more focused electron path at the center. The readout pads under the foil to collect all charges that come through the foil. When an ionizing particle passes through, it produces primary charges by ionization above the electrode, and by means of drift and diffusion processes, the charges are transported through the gas volume to the amplification region close to the electrodes and these charges will attain high velocities due to the high electric field and cause further ionizations leading to an avalanche effect. Separated from the multiplying electrode, the charge collection and readout plane can be patterned at will with strips or pads; usually, they are a set of perpendicular strips to serve as a 2-dimensional projective readout.

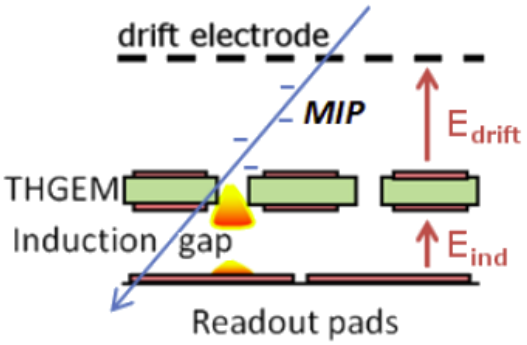

Figure 1.2: Schematic diagram of the Thick-GEM detector setup. Source: [5]

1.4.2 The Micromegas Detector

Micromegas (for MICRO MEsh GAseous Structure) is just like the Thick-GEM, but instead of the Thick-GEM foil that was placed in between the drift electrode and the readout, we now have a very thin micromesh. The working principle is similar to that of the Thick-GEM. In a Micromegas detector, this gas volume is divided in two by a metallic micro-mesh placed, but the multiplication region is very narrow compared to the region above the mesh. This project tries to simulate a calendered mesh and a mesh where the wires are woven into other wires. The results of which are discussed in the subsequent sections.

Chapter 2

The nearly exact Boundary Element Method

As mentioned earlier, in order to simulate microscopic processes we first need the electric field values of the system in consideration. Analytic methods that provide for the same are very accurate although finding such solutions for systems with complex structures can be very difficult. This is where numerical methods like the Finite Element Method (FEM) and Boundary Element Method (BEM) come into the picture.

FEM involves calculating potential at nodes, and the potential value at any other point is obtained using interpolation which can result in inaccuracies. One can increase the number of nodes to reduce the error from inaccuracies but this would need high computational resources or time [6]. FEM also cannot provide enough number of nodes near a tip or sharp surface.

BEM is a numerical implementation of Boundary Integral Method, where the electrode surfaces are divided into regions each of which is assumed to carry a uniform free charge density. The potential at an arbitrary point is calculated by summing the contributions from the charge density (which is calculated by satisfying the Dirichlet/Neumann type boundary conditions for the given device through a suitable Green's function formulation) on each region. But this method cannot produce acceptable results close to geometric singularities (like corners or edge) [7].

Recently, a new approach using analytic expressions for fields, but in the formulation of BEM was proposed, which leads to their nominally exact evaluation [6]. The nearly exact Boundary Element Method (neBEM) solver uses a closed form expressions of the potential and the field obtained from the symbolic integration of the Green's function of a uniform charge density distributed over flat triangular or rectangular boundary element. neBEM first breaks up the system of interest into right triangles and rectangles (they are referred to as primitives) and then the contribution from a primitive (assuming charge is uniformly distributed) is calculated using closed form expressions (analytical solutions) of the potential and the field obtained from the symbolic integration of the Green's function [8]. Unlike BEM, this method is capable of yielding accurate values even in the near-field region.

In the present approach, namely neBEM, the influences are calculated using analytic solution of potential and electrostatic field due to a uniform charge distribution over a flat rectangular surface. The equations of the same are in Ref. [6]. It may be noted here that, in neBEM, any three-dimensional device is assumed to be composed of a number of flat surfaces called primitives. These surfaces can be right-triangular or rectangular. Thus, in the pre-processing stage, the device of interest needs to be segmented into right triangles or rectangles (See Ref. [8]).

If given a uniformly charged rectangle (on the XZ plane) with the two diagonally opposite corners at (x_1, 0, z_1) and (x_2, 0, z_2), Ref. [6] has obtained the closed form expression of the potential at an arbitrary point (X, Y, Z), given by:

$$\begin{aligned}
\phi(X,Y,Z) = &(X-x_1)\ln\left(\frac{D_{12}-(Z-z_2)}{D_{11}-(Z-z_1)}\right)+(X-x_2)\ln\left(\frac{D_{21}-(Z-z_1)}{D_{22}-(Z-z_2)}\right)\\
&+(Z-z_1)\ln\left(\frac{D_{21}-(X-x_2)}{D_{11}-(X-x_1)}\right)+(Z-z_2)\ln\left(\frac{D_{12}-(X-x_1)}{D_{22}-(X-x_2)}\right)\\
&+\frac{\mathrm{i}|Y|}{2}\times\left(S_1\left(\tanh^{-1}\left(\frac{R_1+\mathrm{i}I_1}{D_{11}\,|Z-z_1|}\right)-\tanh^{-1}\left(\frac{R_1-\mathrm{i}I_1}{D_{11}\,|Z-z_1|}\right)\right.\right.\\
&\left.+\tanh^{-1}\left(\frac{R_1-\mathrm{i}I_2}{D_{21}\,|Z-z_1|}\right)-\tanh^{-1}\left(\frac{R_1+\mathrm{i}I_2}{D_{21}\,|Z-z_1|}\right)\right)\\
&+S_2\left(\tanh^{-1}\left(\frac{R_2+\mathrm{i}I_2}{D_{22}\,|Z-z_2|}\right)-\tanh^{-1}\left(\frac{R_2-\mathrm{i}I_2}{D_{22}\,|Z-z_2|}\right)\right.\\
&\left.\left.+\tanh^{-1}\left(\frac{R_2+\mathrm{i}I_1}{D_{12}\,|Z-z_2|}\right)-\tanh^{-1}\left(\frac{R_2-\mathrm{i}I_1}{D_{12}\,|Z-z_2|}\right)\right)\right)-2\pi Y
\end{aligned}\tag{2.1}$$

where $D_{ij}=\sqrt{(X-x_i)^2+Y^2+(Z-z_j)^2}$, $R_i=Y^2+(Z-z_i)^2$, $I_i=(X-x_i)\,|Y|$ and $S_i=\mathrm{sign}\,(z_i-Z)$.

If given a uniformly charged right triangle element (on the XZ plane) with three vertices on (0, 0, 0), (1, 0, 0) and (0, 0, z_M), Ref. [7] has obtained the closed form expression of the potential at an arbitrary point (X, Y, Z), given by:

$$\begin{aligned}
\phi(X,Y,Z) =&12\left(\left(z_MY^2-XG\right)\left(LP_1+LM_1-LP_2-LM_2\right)\right.\\
&+\mathrm{i}|Y|\left(z_MX+G\right)\left(LP_1-LM_1-LP_2+LM_2\right)\\
&-S_1X\left(\tanh^{-1}\left(\frac{R_1+\mathrm{i}I_1}{D_{11}|Z|}\right)+\tanh^{-1}\left(\frac{R_1-\mathrm{i}I_1}{D_{11}|Z|}\right)\right.\\
&\left.\left.-\tanh^{-1}\left(\frac{R_1+\mathrm{i}I_2}{D_{21}|Z|}\right)-\tanh^{-1}\left(\frac{R_1-\mathrm{i}I_2}{D_{21}|Z|}\right)\right)\right)
\end{aligned}\tag{2.2}$$

where D_{ij}, R_i, S_i are the same as ones used in Equation 2.1, $E_1=(X+z_M^2-z_MZ)$, $E_2=(X-1-z_MZ)$, $G=z_M(X-1)+Z$, $H_1=Y^2+G\,(Z-z_M)$, $H_2=Y^2+GZ$,

$LP_1 = \frac{1}{G-\mathrm{i}z_M|Y|}\log\left(\frac{(H_1+GD_{12})+\mathrm{i}|Y|(E_1-z_MD_{12})}{-X+\mathrm{i}|Y|}\right)$, $LM_1 = \frac{1}{G+\mathrm{i}z_M|Y|}\log\left(\frac{(H_1+GD_{12})-\mathrm{i}|Y|(E_1-z_MD_{12})}{-X-\mathrm{i}|Y|}\right)$,
$LP_2 = \frac{1}{G-\mathrm{i}z_M|Y|}\log\left(\frac{(H_2+GD_{21})+\mathrm{i}|Y|(E_2-z_MD_{21})}{1-X+\mathrm{i}|Y|}\right)$ and $LM_2 = \frac{1}{G+\mathrm{i}z_M|Y|}\log\left(\frac{(H_2+GD_{21})-\mathrm{i}|Y|(E_2-z_MD_{21})}{1-X-\mathrm{i}|Y|}\right)$.

One important feature of neBEM, as explained in Ref. [7] is that the results obtained for electrostatic problems containing edges and singularities were numerically stable and physically acceptable, thus showcasing the accuracy, flexibility and robustness of neBEM.

Chapter 3

Simulation Work

Simulations of the Micromegas, Bulk Micromegas and Thick-GEM was done using different geometries in Garfield++ using the neBEM solver. For some results, the same simulations were done using COMSOL Multiphysics® (which is a FEM solver) to compare plots obtained using neBEM.

The main interest of these simulations were with respect to the Micromegas detector with the calendared meshes. The objective of simulating the Micromegas detector (and different calendared meshes) was to purchase one of these meshes to use in an experiment to be conducted at Saha Institute of Nuclear Physics, Kolkata. We also sought to find the expected gain and signals in the best mesh configuration. This process also involved studying the drift lines produced for an incoming muon or electron.

3.1 Electric Field Calculations for a Thick-GEM Detector

All plots shown in this section are for a Thick-GEM detector with the following specifications:

1. Thick-GEM foil made of Kapton and Copper.
2. Inner and outer hole diameter = 0.3mm and 0.4mm respectively.
3. Thickness of Kapton and Copper in Thick-GEM foil = 0.4mm and 5μm respectively.
4. Thickness of drift electrode and anode = 5μm.
5. Pitch = 1mm.
6. Induction and drift gap = 1mm.

7. Voltages given to the drift electrode, upper Thick-GEM layer, bottom Thick-GEM layer and anode = -750V, -250V, 250V, and 750V respectively.

8. A Thick-GEM with a total of 50 holes was simulated, unless stated otherwise.

3.1.1 Qualitative Comparison of neBEM and COMSOL Multiphysics® Results

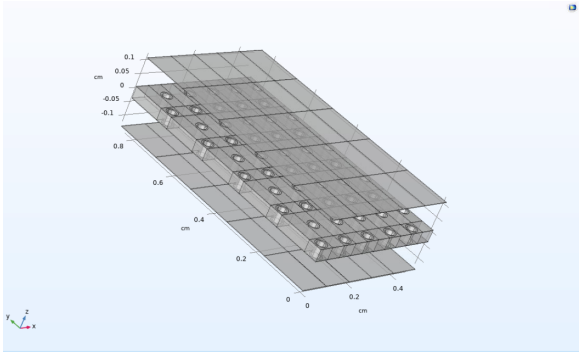

(a)

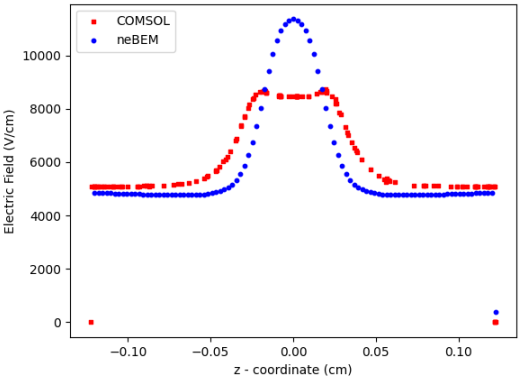

(b)

Figure 3.1: (a) The Thick-GEM detector as built in COMSOL Multiphysics® and (b) a plot of the electric field across a line passing through the center of a hole obtained using neBEM and COMSOL Multiphysics®.

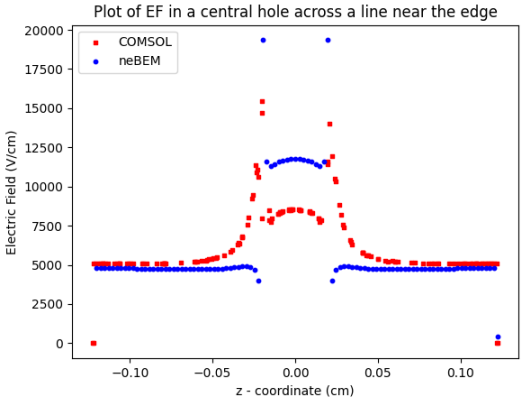

Figure 3.2: Plots of the electric field across a line passing through a hole at the center of the foil close to the hole wall. It compares neBEM and COMSOL Multiphysics®.

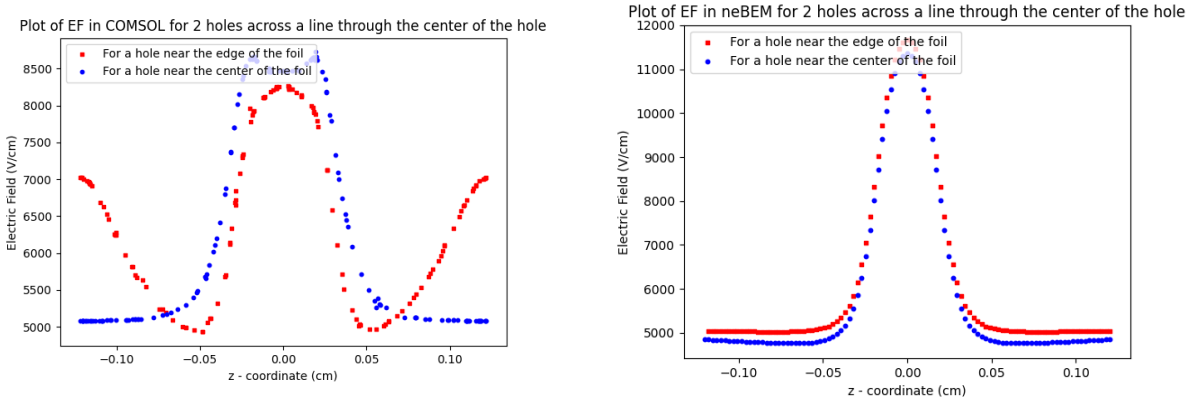

(a) (b)

Figure 3.3: Plots of the electric field across lines passing near the hole wall, for 2 holes, one at the center of the foil and the other near the edge of the foil to look at edge effects. Plots (a) and (b) were done using COMSOL Multiphysics® and neBEM respectively.

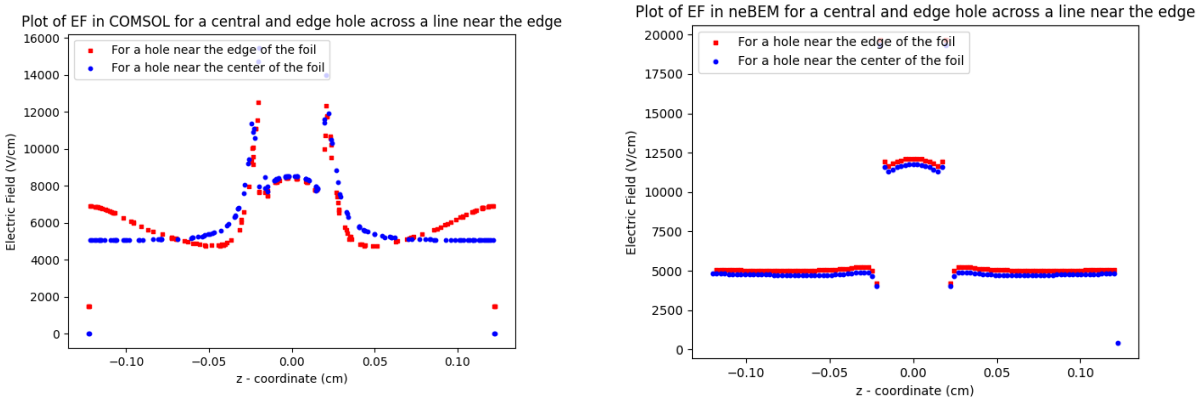

(a) (b)

Figure 3.4: Plots of the electric field across lines passing through the center of the hole, for 2 holes, one at the center of the foil and the other near the edge of the foil to look at edge effects. Plots (a) and (b) were done using COMSOL Multiphysics® and neBEM respectively.

From the above figures we see that there is a difference between results obtained using neBEM and COMSOL Multiphysics® in magnitude and trends. From Figures 3.3a, 3.3b, 3.4a and 3.4b, we observe some kind of effects induced at the edge, and also the differences between neBEM and COMSOL Multiphysics® results at different regions of the detector foil.

3.1.2 Effects of Different Parameters

There are a variety of parameters that we can control while running simulations in COMSOL Multiphysics® and neBEM. The parameters we studied for neBEM are target element sizes (which give rise to different discretizations), number of panels, number of Thick-GEM holes, Periodic Boundary Conditions (PBCs), etc. We vary the number of Thick-GEM holes to reach a good position in the computation-accuracy trade-off as we would like to know how many holes we need to simulate, beyond which the values of the electric field saturate. While choosing the number of repetitions, we need to keep in mind that the resulting extent is large enough to satisfy parallel plate conditions at the center of the device.

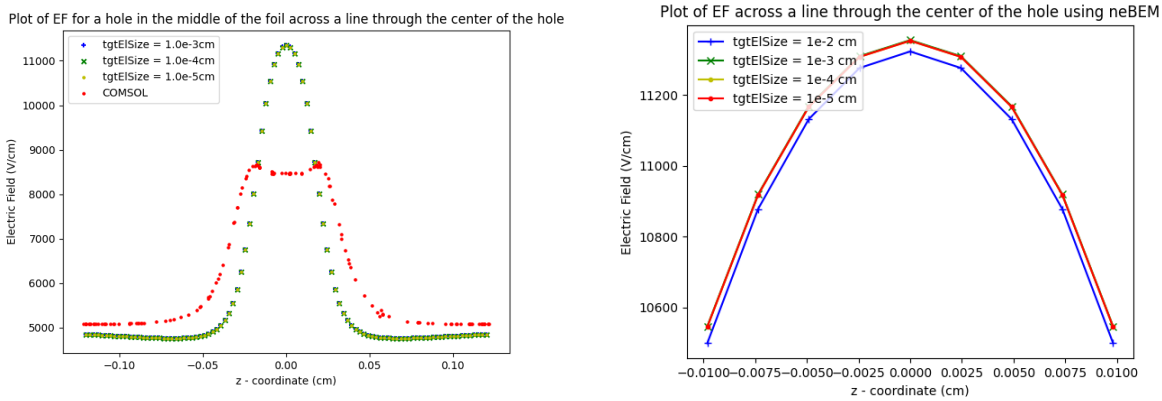

(a) (b)

Figure 3.5: Plots of the electric field vs Z-coordinate obtained using neBEM for different target element sizes across a line (a) through the entire height of the detector volume (also with a plot from COMSOL Multiphysics® for comparison) and (b) near the foil-region.

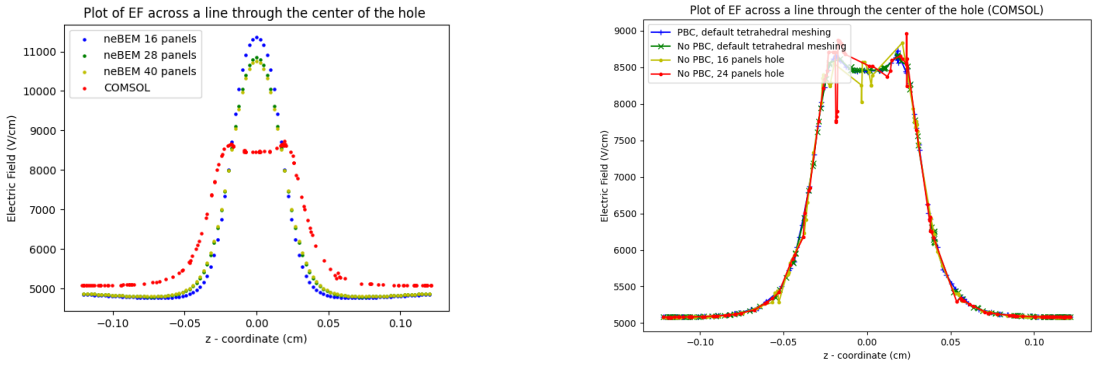

(a) (b)

Figure 3.6: Plots of the electric field vs Z-coordinate obtained using (a) neBEM for different panels (also with a plot from COMSOL Multiphysics® for comparison) and (b) COMSOL Multiphysics® for different conditions like panel numbers, tetrahedral meshing and PBC.

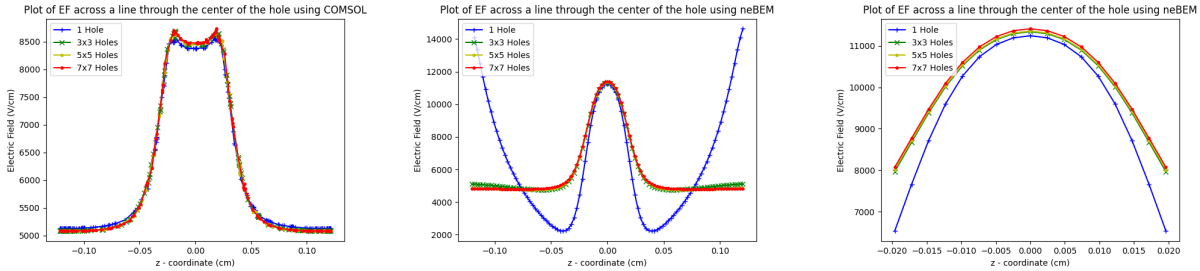

(a) (b) (c)

Figure 3.7: Plots of the electric field vs Z-coordinate obtained for different Thick-GEM unit cell repetitions using (a) COMSOL Multiphysics®, (b) neBEM and (c) neBEM but near the foil-region.

One observation we can make from Figure 3.7a is that despite changing multiple parameters, the obtained field values are still similar in COMSOL Multiphysics®.

3.2 Electric Field Calculations for the Micromegas Detector

Simulation were done for Micromegas with a calendared mesh and a bulk Micromegas with a mesh where wires go through each other. The specifications of the same are as follows:

Detector	Mesh wire diameter (μm)	Gap between mesh wires (μm)	Amplification gap (μm)	Drift gap (cm)
Micromegas	80	120	300	1.2
	28	36	300	1.2
	40	62	300	1.2
Bulk Micromegas	18	45	192	1.3

Table 3.1: Specifications of the Micromegas and bulk Micromegas detectors that were simulated.

The voltages given to the drift electrode, mesh and anode were -1000V, -700V and 0V respectively. We will refer to each configuration as Micromegas/ bulk Micromegas using the notation (mesh wire diameter, gap between mesh wires). For example the first row of Table 3.1 will be referred to as the (80,120) configuration. The XY plane is the mesh plane.

3.2.1 The Micromegas Detector (With a Calendared Mesh)

The structure of the detector is a standard one, except that the mesh has calendared-like weaves. In neBEM (and COMSOL Multiphysics®), this was implemented through 3 designs. The images of the unit cells these designs of the meshes are as follows:

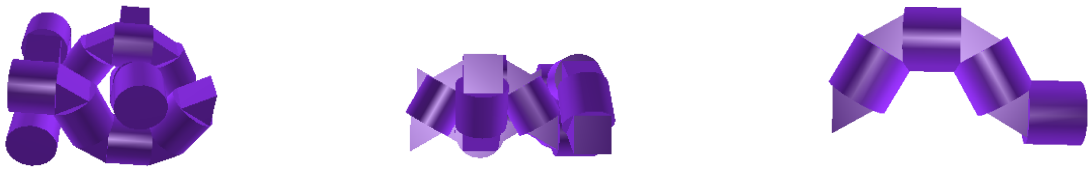

(a) (b) (c)

Figure 3.8: (a), (b) Unit cells of the meshes made. (c) A single wire of the unit cell of the mesh. These images correspond to Design 1.

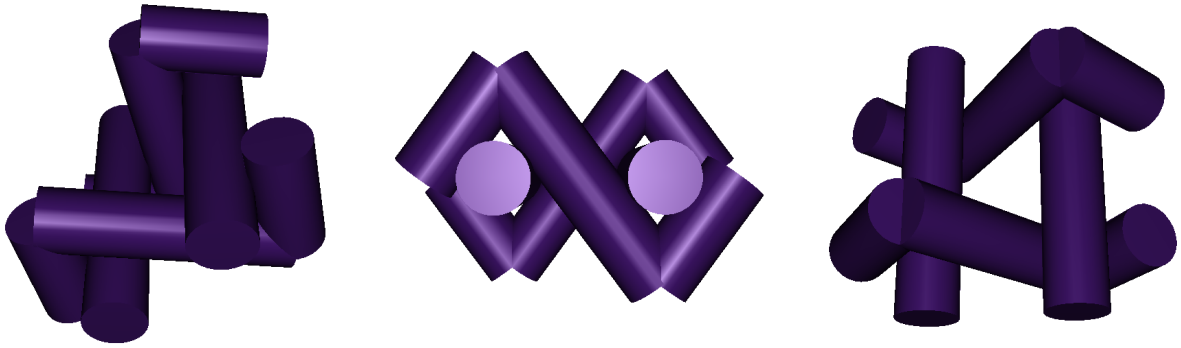

(a) (b) (c)

Figure 3.9: Unit cells of the meshes made. These images correspond to Design 2.

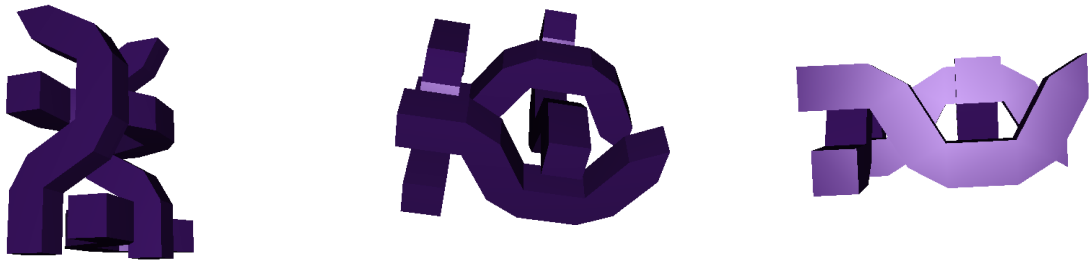

(a) (b) (c)

Figure 3.10: Unit cells of the meshes made. These images correspond to Design 3.

The electric field plots were look at, only for Design 1, and reasons for this will be explained later.

For the results that follow, unless stated otherwise, we use 9 copies of the unit cell along x and y axes as a default value. For Design 1, the plots for the 3 mesh configurations (refer Table 3.1) are as shown in the following figures:

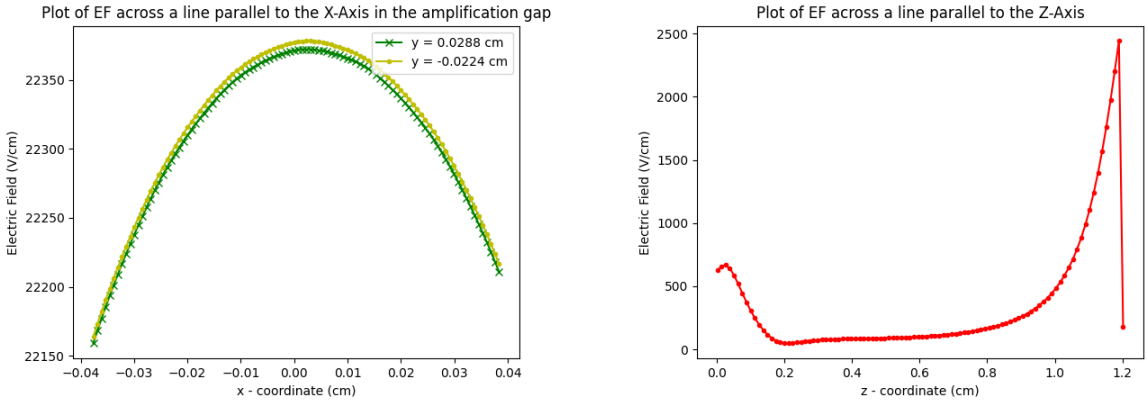

(a) (b)

Figure 3.11: The above plots are for Design 1, (28, 36) configuration. Plots for the electric field (a) across a line parallel to the X-axis but at different Y-coordinates in the amplification region and (b) across a line along the Z-axis.

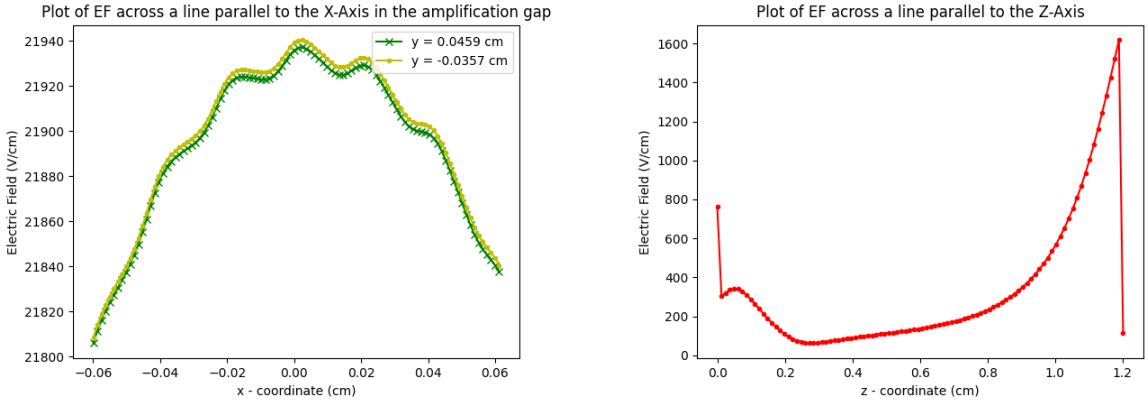

(a) (b)

Figure 3.12: The above plots are for Design 1, (40, 62) configuration. Plots for the electric field (a) across a line parallel to the X-axis but at different Y-coordinates in the amplification region and (b) across a line along the Z-axis.

Figures 3.11a, 3.12a and 3.13a do not provide any inference with respect different y-coordinates being used, they were made to show electric field fluctuations between the mesh configurations.

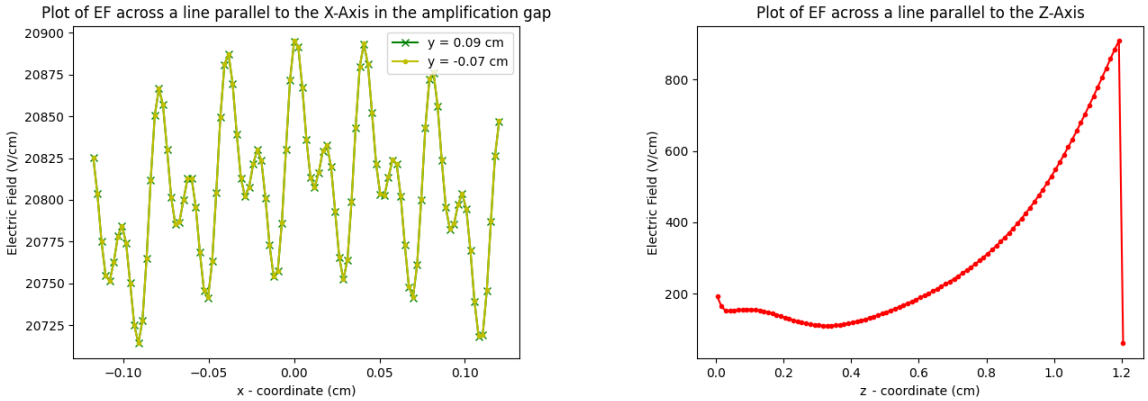

(a) (b)

Figure 3.13: The above plots are for Design 1, (80, 120) configuration. Plots for the electric field (a) across a line parallel to the X-axis but at different Y-coordinates in the amplification region and (b) across a line along the Z-axis.

From the above plots, we can see that the (28, 36) configuration seems to display stably-changing electric fields. Further plots made to study this configuration are as shown below:

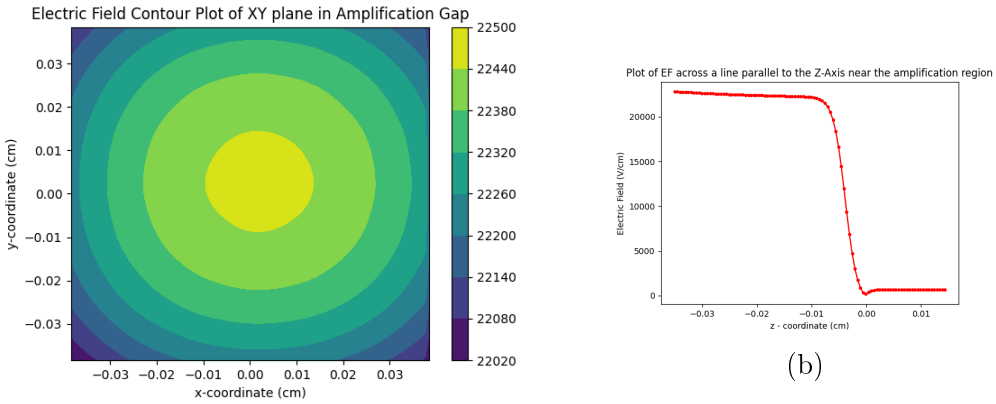

(a) (b)

Figure 3.14: The above plots are for Design 1, (28, 36) configuration. (a) The electric field contour plot of the XY plane at a Z-coordinate in the amplification region. (b) Plots of the electric field across a line along the Z-axis but only in the amplification region.

From Figure 3.15a we can see that as we go towards the mesh, the fields start to fluctuate a bit. And from Figure 3.15b it is evident that for different periodic copies of the unit cell, there are edge effects involved. As explained in Section 3.1.2, we can use such plots to determine the number of periodic copies we need to use to remove edge effects, while still saving on some computation time.

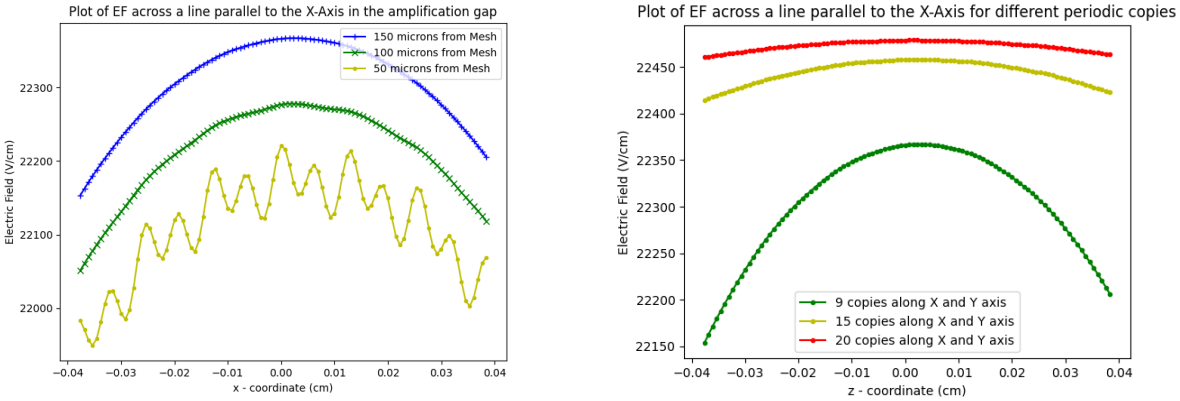

(a) (b)

Figure 3.15: The above plots are for Design 1, (28, 36) configuration. Plots for the electric field across a line parallel to the X-axis (a) for different heights (Z-axis) in the amplification region and (b) for different number periodic copies of the unit cell

After subsequent discussion, the group came to a conclusion that the (28, 36), with an opening area of 31.25% is the best mesh to procure. To that effect we went forward to perform gain and signal calculations in this configuration.

Although the study of neBEM and COMSOL Multiphysics® was done in previous sections for the Thick-GEM detector. and that the objective of this section is different, we still were curious with how results fared between the two for this detector. The results of the comparison are as follows:

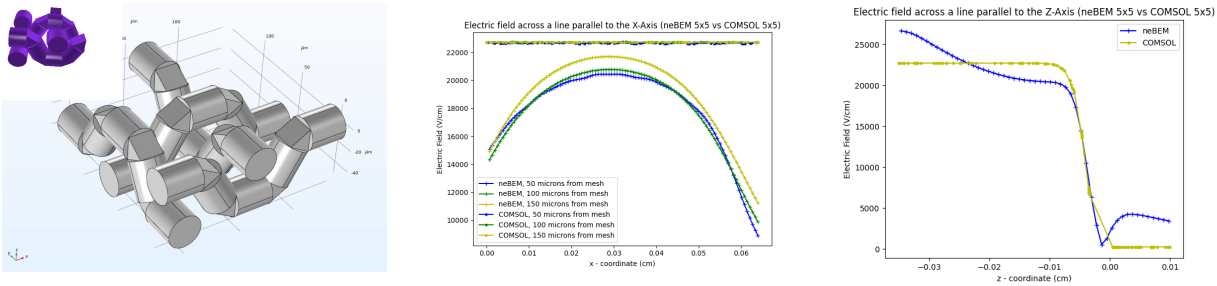

(a) (b) (c)

Figure 3.16: (a) An image showing the comparison of the unit cells made in neBEM (in purple) and COMSOL Multiphysics®. Plots of the electric field values obtained using neBEM and COMSOL Multiphysics® across lines along the X-axis (b) for different Y-coordinates and (c) for different heights (Z-axis) in the amplification region.

We then started to plot drift lines in the detector for an incoming ionizing radiation. But

Design 1 was not giving any standard results, i.e, we saw no avalanche effect or even a decent amount of multiplication for an incoming electron of energy 5keV. We were getting a gain of about 5 electrons, which is not even close to the right order of gain. There were instances where we got outputs as shown in Figure 3.17. For this reason, we started making other designs to see if the reason for such results were from multiple sharp edges present in Design 1. Thus came Designs 2 and 3 to provide for a simpler and smooth structure respectively. neBEM failed to discretise the geometry in Design 2, for which we had to drop that design. We then plotted figures similar to the ones previously shown in this section and we observed that the electric field plots of Design 1 and 3 were similar, so we went forward with gain calculations while assuming the electric field plots made for Design 1 would be the same as Design 3.

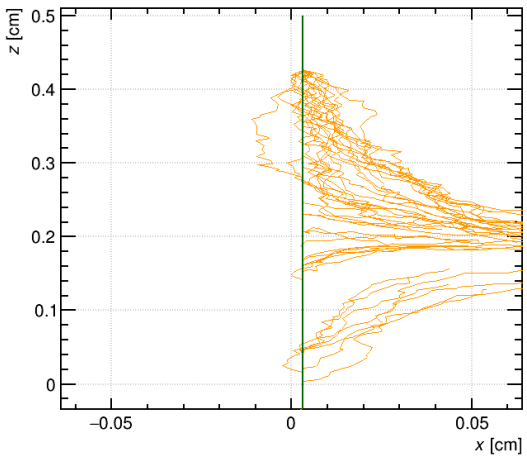

Figure 3.17: The drift lines obtained for an incoming electron of energy 5keV in Design 1.

Looking into Design 3, we see that the unit cell is not symmetric around the center of the cell, so we went ahead to make a minor change to make the design of the unit cell as symmetric as possible. The previous unit cell was also not centered at the origin, so we also modified the code so that the center of the unit cell and the origin is aligned. The new unit cell and results obtained for the same are as follows:

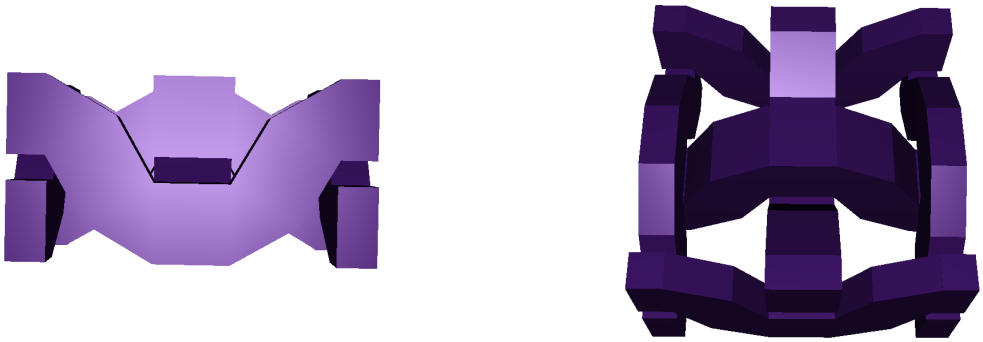

Figure 3.18: Unit cells of the modified mesh of Design 3.

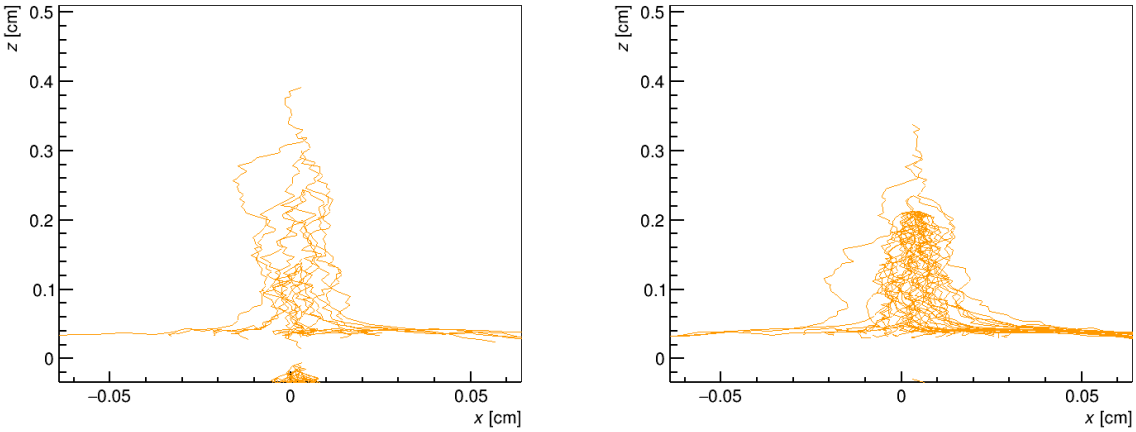

(a) (b)

Figure 3.19: The drift lines obtained for Design 3 for an incoming muon of energy 1GeV.

We see that the modifications made to Design 3 helped in producing better drift lines as compared to the previous version. At this stage, we realized there was some bug in the code, but another slight modification with the size of the unit cell helped in producing the desired results:

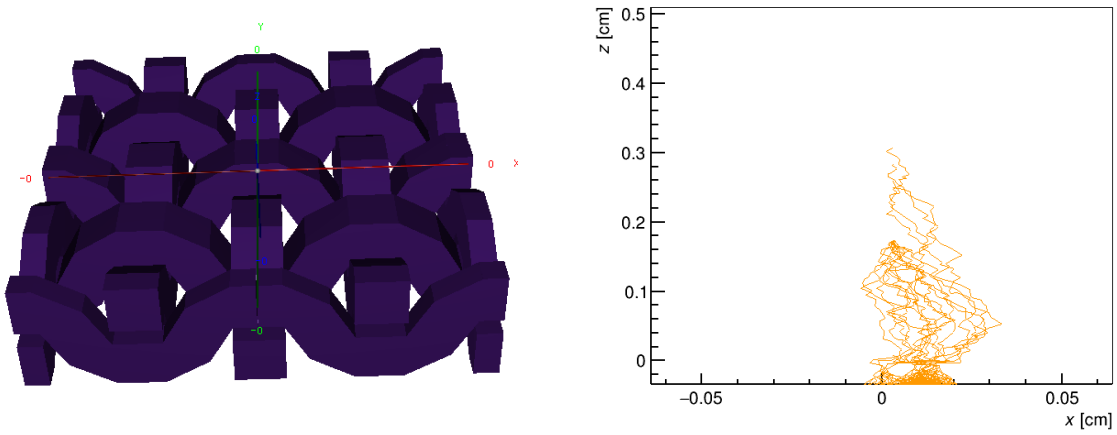

(a) (b)

Figure 3.20: The unit cells of the modified mesh of Design 3 that was used and (b) the drift lines obtained for the subsequent design for an incoming muon of energy 1GeV.

3.2.2 The Bulk Micromegas Detector

The schematic diagram of the mesh unit cell of the bulk Micromegas is as follows:

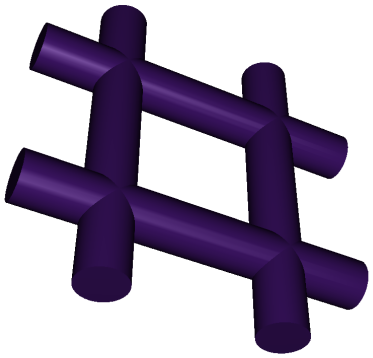

Figure 3.21: A diagram of the mesh's unit cell of the bulk Micromegas detector.

We simulated the (18, 45) bulk Micromegas to obtain the following plots:

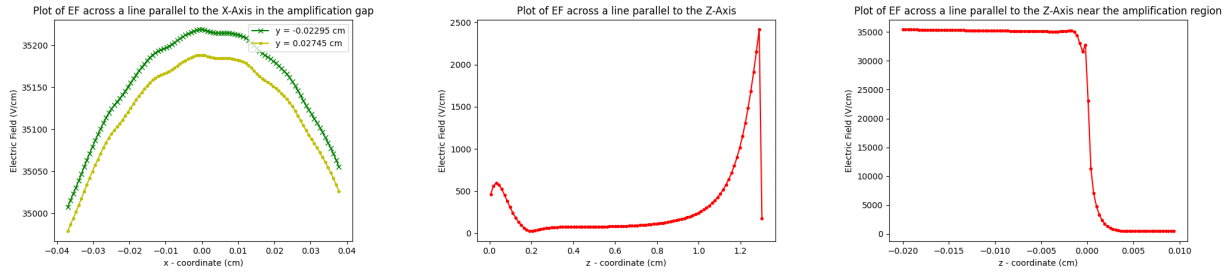

(a) (b) (c)

Figure 3.22: Plots of the electric field values for the (18,45) bulk Micromegas (a) across lines along the X-axis for different Y-coordinates, across a line along the (b) Z-axis and (c) Z-axis but only in the amplification region.

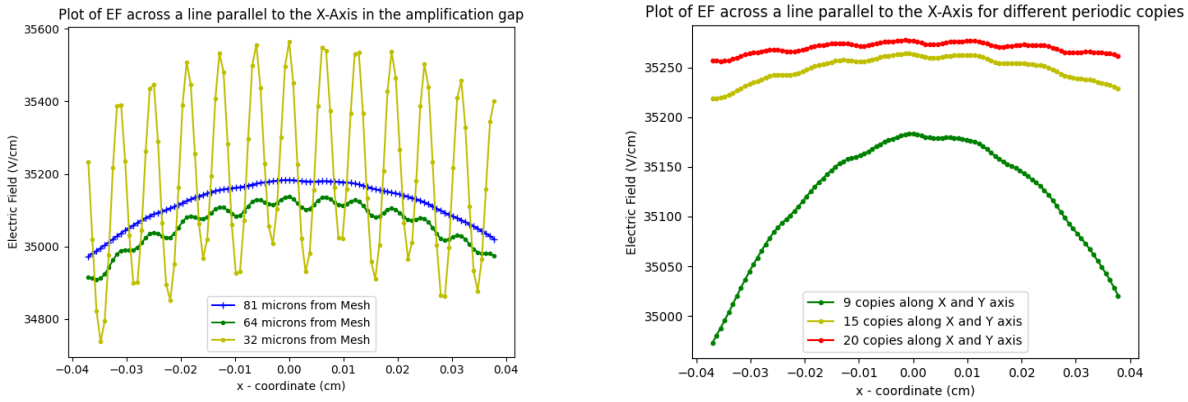

(a) (b)

Figure 3.23: Plots for the electric field across a line parallel to the X-axis (a) for different heights (Z-axis) in the amplification region and (b) for different number periodic copies of the unit cell

From Figure 3.23a we can see that as we go towards the mesh, the fields start to fluctuate a bit. And from Figure 3.23b it is evident that for different periodic copies of the unit cell, there are edge effects involved. Similar to what was discussed for the (28, 36) configuration of the Micromegas detector, we can use such plots to determine the number of periodic copies we need to use to remove edge effects, while still saving on some computation time.

3.2.3 The Micromegas Detector With a Smooth Calendared Mesh in COMSOL Multiphysics®

The previous attempts for simulating the calendared mesh involved making the mesh using the structures available to us in neBEM, which were mostly primitive shapes like cuboids and cylinders. We attempted to simulate a smooth and realistic mesh in COMSOL Multiphysics®.

We first made a unit cell and produced periodic copies to obtain electric field values, (we first simulated with 3 copies along the X and Y directions). The images of the unit cells and the results of the simulations for the same are shown below:

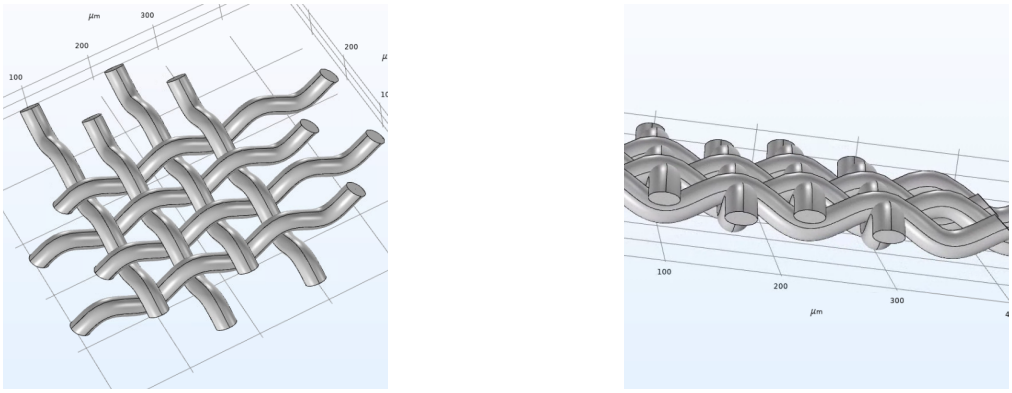

(a) (b)

Figure 3.24: Sample images of a bigger mesh made in COMSOL Multiphysics®.

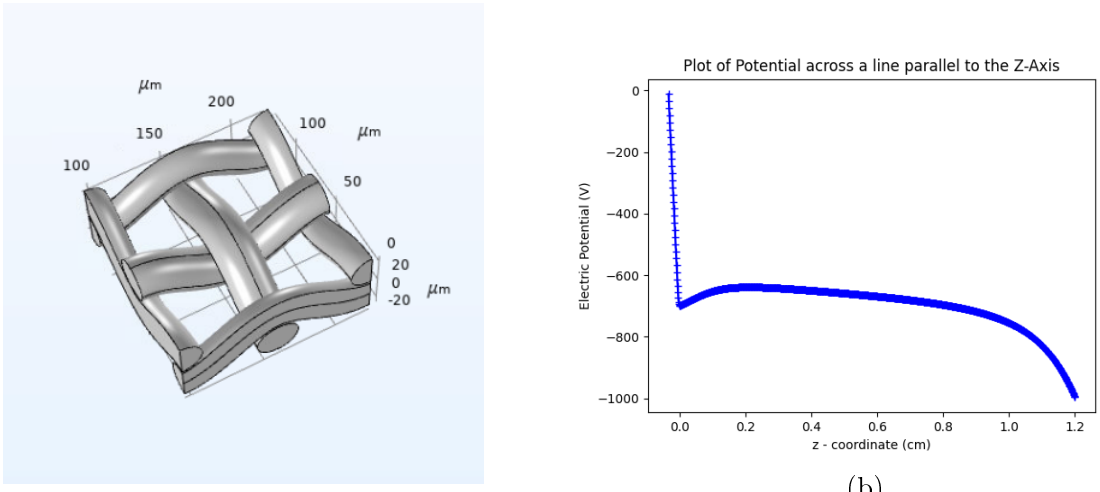

(a) (b)

Figure 3.25: (a) Image of the unit cell used. (b) Plot of the electric potential for the same.

The main issue that we faced was computation time. As we increased the number of copies of the unit cell, the computation time increased drastically, which prevented us to perform further simulations in COMSOL Multiphysics® for this smooth mesh. While choosing the number of repetitions, we need to keep in mind that the resulting extent should be large enough to satisfy parallel plate conditions at the middle of the device, but owing to time taken to perform such tasks, we could not proceed in this direction.

COMSOL Multiphysics® has a PBC feature using which we need not make periodic copies of the unit cell, but obtain parallel plate conditions. We did attempt using PBCs to simulate the same, but we were not able to proceed further in this direction too, as the mesh was made by sweeping a 2-dimensional circle onto a 2-dimensional sine wave. This meant that on opposite ends of the unit cell, the mesh endings might not exactly match, and more precisely, the node coordinates on opposite ends need to be mirroring in order to be able to use PBC, which was not possible with crude design.

Chapter 4

Summary

During the entirety of the project, fundamentals of gaseous radiation detectors and the neBEM solver was learned. The skills pertaining to simulating electric field lines and drift lines of a gaseous detector using Garfield++ (through the neBEM library) and COMSOL Multiphysics® was learned. The simulations performed during the project and subsequent remarks are as follows:

1. The Thick-GEM detector was simulated using neBEM and COMSOL Multiphysics®, and the obtained results were compared.

2. For the Thick-GEM detector, we also studied the effects of changing parameters like target element size, number of panels, periodic boundary conditions, meshing etc.

3. We studied three different calendared mesh configurations for the Micromegas detector to help with the decision of procuring one of these meshes for a future experiment. Multiple studies were performed in this part, including number of unit-cell repetitions to satisfy parallel plate conditions at the center of the device, variation of the electric field near the mesh, and comparison of neBEM and COMSOL Multiphysics® electric field plots.

4. After deciding the best mesh configuration, we successfully were able to obtain the plot of the drift lines for an incoming muon.

5. A bulk Micromegas detector was also simulated and electric field plots for the same were obtained.

6. Simulation of a smooth and realistic calendared mesh in COMSOL Multiphysics® was done through repeated unit cells, but we were not able to simulate the same using periodic boundary conditions owing to reasons explained in Section 3.2.3.

Chapter 5

Outlook

Owing to time considerations, a full-fledged study could not be done. As we progressed through the project, there were multiple realizations of the directions of work that this project can go into. They are explained in the following points:

1. neBEM and COMSOL Multiphysics® results were although similar, but not fully exact. One can look into this direction to figure out how can neBEM be improved to obtain results comparable to the industry-standard COMSOL Multiphysics® software.

2. We were not able to use periodic boundary conditions for the smooth and realistic calendared mesh. Work can be done in this direction using better mesh designs and meshing settings of COMSOL Multiphysics®.

3. Important observations that was found unexplained were the considerations like origin of the unit cell, symmetric nature of the unit cell, etc that one needs to keep in mind while simulating a system using periodic copies in the neBEM framework. We saw that the center of the unit cell is an important factor to simulate, and also that the unit cell should be symmetric to get correct results. There is also a possibility of a bug in the neBEM code along the same directions. A very important study can be dedicated into looking at such aspects.

4. In the given time, we were able to reach only until simulating the drift lines. More work can be done to fully finish this project by performing more studies on the gain and signal calculations for the mesh configurations we looked into.

Bibliography

[1] William R. Leo. *Techniques for nuclear and particle physics experiments: a how-to approach*. Springer, 2nd rev. ed edition, 1994. ISBN: 9783540572800,3540572805,0387572805. URL: http://gen.lib.rus.ec/book/index.php?md5=fbd221f7f73ebf68ffd16d7c438c93fb.

[2] Meek J. M. and Cragg J.D. *Electrical Breakdown Of Gases*. The International Series of Monographs on Physics. Oxford (Clarendon Press), 1953.

[3] Sumanya Sekhar Sahoo. Study of gaseous detectors for high energy physics experiments, National Institute of Science Education and Research, 2015.

[4] F. Sauli. *Gaseous Radiation Detectors: Fundamentals and Applications*. Cambridge Monographs on Particle Physics, Nuclear Physics and Cosmology. Cambridge University Press, 2014. ISBN: 9781107043015.

[5] S Bressler, L Arazi, L Moleri, M Pitt, A Rubin, and A Breskin. Recent advances with thgem detectors. *Journal of Instrumentation*, 8(12):C12012–C12012, December 2013. ISSN: 1748-0221. DOI: 10.1088/1748-0221/8/12/c12012. URL: http://dx.doi.org/10.1088/1748-0221/8/12/C12012.

[6] N. Majumdar and S. Mukhopadhyay. Simulation of three-dimensional electrostatic field configuration in wire chambers: a novel approach. *Nuclear Instruments and Methods in Physics Research Section A: Accelerators, Spectrometers, Detectors and Associated Equipment*, 566(2):489–494, 2006. ISSN: 0168-9002. DOI: https://doi.org/10.1016/j.nima.2006.06.035. URL: https://www.sciencedirect.com/science/article/pii/S0168900206011703.

[7] Supratik Mukhopadhyay and Nayana Majumdar. A study of three-dimensional edge and corner problems using the nebem solver. *Engineering Analysis with Boundary Elements*, 33(2):105–119, 2009. ISSN: 0955-7997. DOI: https://doi.org/10.1016/j.enganabound.2008.06.003. URL: https://www.sciencedirect.com/science/article/pii/S0955799708001045.

[8] N Majumdar, S Mukhopadhyay, and S Bhattacharya. 3d field simulation in GEM-type structures. *Journal of Instrumentation*, 4(10):P10013–P10013, October 2009. DOI: 10.1088/1748-0221/4/10/p10013. URL: https://doi.org/10.1088/1748-0221/4/10/p10013.